Journal of Catalysis 298 (2013) 138–147

Contents lists available at SciVerse ScienceDirect

Journal of Catalysis

journal homepage: www.elsevier.com/locate/jcat

An effective heterogeneous L-proline catalyst for the direct asymmetric aldol reaction using graphene oxide as support

Rong Tan [a], Chengyong Li [a], Jianqing Luo [a], Yu Kong [a], Weiguo Zheng [a], Donghong Yin [a,b,*]

[a] Key Laboratory of Chemical Biology and Traditional Chinese Medicine Research (Ministry of Education), Hunan Normal University, Changsha, Hunan 410081, China
[b] Technology Center, China Tobacco Hunan Industrial Corporation, No. 426 Laodong Road, Changsha, Hunan 410014, China

ARTICLE INFO

Article history:
Received 1 September 2012
Revised 23 October 2012
Accepted 19 November 2012

Keywords:
L-Proline
GO sheet
Chiral heterogeneous catalyst
Direct asymmetric aldol reaction
Enantiomeric selectivity

ABSTRACT

Pristine L-proline was non-covalently loaded on the graphene oxide (GO) sheet in a simple route by mixing them in aqueous solution. Technologies of characterization well suggested that L-proline was efficiently loaded on the two sides and edge of the GO sheet through hydrogen-bonding or/and ionic interaction, giving the excellent **L-proline/GO** hybrid catalyst for the direct asymmetric aldol reaction. The unique multilayered structure of the GO carrier with sufficient interlayer space favored reagents' diffusion toward L-proline chiral moiety and therefore resulted in the high catalytic efficiency of the heterogeneous L-proline. Excellent yield (96%) with high enantiomeric excess (79% *ee*) was obtained in the direct aldol reaction of 2-nitrobenzaldehyde with acetone catalyzed by **L-proline/GO** hybrid, which was comparable to that observed in the reactions promoted by L-proline itself. Furthermore, the **L-proline/GO** hybrid used as a heterogeneous catalyst could be easily recovered and recycled for seven times without significant loss of the reactivity.

1. Introduction

The direct asymmetric aldol reaction is one of the most important C—C bond-forming reactions in organic synthesis and is of much importance in the pharmaceutical, agrochemical, and fine chemical industries [1–4]. In 2000, List et al. demonstrated the use of proline as an efficient catalyst for the direct asymmetric aldol reaction between unmodified ketone and a variety of aldehydes [5]. The proline used as an important chiral small-molecule organocatalyst has been drawn much attention since it is easily accessible, environmentally safe, and available in both the enantiomeric forms [6–8]. However, it suffered from the unavoidable drawbacks of homogeneous catalytic processes (e.g., lower thermal stability and difficulties in catalyst separation and recovery). Immobilization and recycling of L-proline have received considerable concerns in recent years. Several types of supports, such as polymer [9–12], silica [13–17], ionic liquid (IL) [18,19], β-cyclodextrin [20], Merrifield resin [21] and magnetite [22], are usually considered for the immobilizations of proline and its derivatives. Gruttadauria and his co-workers [9–11] used polystyrene-supported proline-based organic catalysts for the direct asymmetric aldol reaction. Zou et al. [12] investigated the catalytic behaviors of PVC-TEPA-supported L-proline in the aldol reaction. Lu et al. [13] synthesized L-proline-functionalized polymers as supported organocatalysts. Bae et al. [14,15] grafted L-proline onto the heterogenized silica for catalyzing the asymmetric aldolization. Calderón et al. [16,17] catalyzed the asymmetric aldol reaction by proline on mesoporous materials. Miao and Chan [18] prepared an IL-anchored proline catalyst, which was efficient and recyclable for asymmetric aldol reaction. The heterogeneous catalysts indeed can be recycled for reuse, but some of them are less efficient due to the low accessibility of substrates. Recently, layered double hydroxides (LDHs) have emerged as an attractive support to develop the L-proline/LDHs hybrid using intercalation of L-proline in Mg—Al LDH through ion-exchange method [23]. It is found that the immobilization of L-proline on LDHs has no adverse effect on the catalytic activity of L-proline. Thus, this represents a fascinating strategy for developing the heterogeneous L-proline catalyst with high efficiency and easy reusability by supporting the L-proline on layered materials.

Recently, a newly layered material-graphene oxide (GO) has attracted much attention of scientists all over the world, since it exhibits unique surface properties (oxygenated functional groups on the basal planes and edge), high-specific surface area, and easy exfoliation into monolayers under water [24–26]. In particular, the GO consists of intact graphitic regions interspersed with sp^3-hybridized carbons containing carboxyl, hydroxyl, and epoxide functional groups on the edge, top, and bottom surface of each sheet and sp^2-hybridized carbons on the aromatic network [26].

* Corresponding author at: Key Laboratory of Chemical Biology and Traditional Chinese Medicine Research (Ministry of Education), Hunan Normal University, Changsha, Hunan 410081, China. Fax: +86 731 88872531.
E-mail address: yindh@hunnu.edu.cn (D. Yin).

0021-9517/$ - see front matter © 2012 Elsevier Inc. All rights reserved.
http://dx.doi.org/10.1016/j.jcat.2012.11.024

The presence of the abundant oxygen functional groups provides GO sheet with large capability of loading organic molecules through covalent or non-covalent approaches, facilitating development of a broad novel class of materials with enhanced properties and even introducing new functionalities to GO sheet [27,28]. Yang et al. have reported high-efficiency loading of doxorubicin hydrochloride (DXR) on GO sheet (0.91 mg/mg) through hydrogen-bonding interaction between GO and DXR, as well as the π–π stacking interaction [29]. Apart from the abundant oxygen functional groups, the key to understanding the large loading capability of GO sheet lies in the large theoretical specific surface area (up to 400–1500 $m^2 g^{-1}$) [30], as well as the high efficient utilization of surface area because both sides of the nanosheet are accessible.

Based on the fascinating layered structure of GO material, as well as the large capability of loading organic molecules, we reason that the GO can be used as an efficient support for L-proline and allows for desirable catalytic properties. It is well known that the carboxyl and secondary amine groups of the L-proline are capable of participating in hydrogen bond [31], and we thus decide to introduce the L-proline into the GO sheet through the hydrogen-bonding interaction between the L-proline and the GO sheet to prepare the **L-proline/GO** hybrid. We envision that the GO sheet can efficiently load L-proline molecular on its two sides and edge, resulting in a sandwich-like hybrid (**L-proline/GO**) where layers of GO sheet alternate with layers of L-proline. The intercalated L-proline component serves as the catalytic sites, and the GO sheet as support is expected to favor accessibility of reagents, which in turn increases the catalytic efficiency of the heterogeneous L-proline catalyst. Furthermore, the non-covalent method, which does not need to tune the structures of the L-proline and the GO sheet, represents an interesting strategy for the attachment of active sites on the GO sheet for use in catalytic reactions. Herein, L-proline was efficiently loaded on GO sheet simply by using the non-covalent approach. It is interesting that the layered **L-proline/GO** hybrid, in which reagents can free access interlamellar space, functions as the heterogeneous catalyst, but behaves as the homogeneous catalyst. Thus, it presents comparable catalytic activity and enantioselectivity relative to the pristine L-proline and can be easily separated for reuse by centrifugation.

2. Experimental

2.1. Materials and methods

4-nitrobenzaldehyde, 2-chlorobenzaldehyde, and 4-acetamidobenzaldehyde were obtained by TCI. 2-nitrobenzaldehyde, 2-naphthaldehyde and 4-bromobenzaldehyde were bought from Acros. 3-pentanone, cyclohexanone, and cyclopentanone were purchased from Aldrich. Other commercially available chemicals were laboratory grade reagents from local suppliers. They were used without further purification, except for the aromatic aldehyde, which was purified by distillation.

^{1}H NMR spectra of samples were recorded at a Varian-500 spectrometer. Tapping mode atomic force microscopy (AFM) measurements were performed using a multimode SPM from Digital Instruments with a Nanoscope IIIa Controller. X-ray diffraction (XRD) patterns were recorded on a Philips X'PERT-Pro-MPD diffractometer using Cu K_α radiation (λ = 1.542 Å). A continuous scan mode was used to collect 2θ from 5° to 40°. Fourier transform infrared (FT-IR) spectra were obtained as potassium bromide pellets with a resolution of 4 cm^{-1} and 32 scans in the range 400–4000 cm^{-1} using an AVATAR 370 Thermo Nicolet spectrophotometer. Elemental analyses of N were carried out on Vario EL III Elemental analyses made in Germany. The thermogravimetric and differential thermogravimetric (TG–DTG) analysis was performed on Netsch STA449c. The sample weight was *ca.* 10 mg and was heated from room temperature up to 800 °C with 10 °C/min using alumina sample holders. Analytical high performance liquid chromatography (HPLC) was carried out on Waters 2695 Separations Module with Waters 2996 photodiode array detector using Daicel chiralpak OB-H, AD-H or AD columns.

2.2. Preparation of L-proline/GO hybrid

In the experiments, GO was prepared by the oxidation of high-purity graphite powder (99.9999%, 200 mesh) with H_2SO_4/$KMnO_4$ according to the method of Hummers and Offeman [32]. After repeated washing of the resulting yellowish-brown cake with hot water, the powder of GO was dried at room temperature under vacuum overnight. FT-IR (KBr): 3390, 3132, 1735, 1621, 1224, 1050, 581 cm^{-1}.

The mixture of the dried GO (0.1 g) and L-proline (0.2 g) was sonicated in deionized water for 0.5 h and further stirred at room temperature for 24 h. After centrifugal separation by using an Eppendorf 5804 centrifuge operated at 10,000 rpm for 15 min, the precipitate was collected and dried overnight under vacuum to give brown flake solid of **L-proline/GO** hybrid. FT-IR (KBr): 3369, 2976, 2741, 2301, 1617, 1398, 1326, 1163, 1036, 837, 775, 673, 620 cm^{-1}. The L-proline content in the **L-proline/GO** hybrid is 4.06 mmol/g, which was determined according to the content of nitrogen element in **L-proline/GO** hybrid analyzed by elemental analyses.

For comparison, we also prepared the graphite-supported L-proline catalyst (L-proline/graphite) and the active carbon-supported L-proline catalyst (L-proline/AC) according to the above similar preparation procedure. L-proline content in the prepared catalysts was also measured in terms of nitrogen element percentage as obtained from nitrogen elemental analyses results. The results are listed in Table 1.

2.3. General procedure for the direct asymmetric aldol reaction

2.3.1. Typical procedure for the asymmetric aldol reactions of acetone with various aryl aldehydes

A mixture of catalyst (0.035 g, 0.14 mmol L-proline content in the **L-proline/GO** hybrid) and acetone (4 ml) was stirred at 30 °C for 10 min. Subsequently, the corresponding aromatic aldehyde (0.5 mmol) was added. The resulting mixture was stirred at room temperature until the reaction was judged to be complete based on TLC analysis. The catalyst was then separated by centrifugation. The upper organic phase with the product was concentrated under reduced pressure. The crude products were purified by column chromatography on silica gel (Acros, 40–60 μm, 60 Å, eluent hexane/ethyl acetate 5:1). Enantiomeric excess (*ee* value) was determined by HPLC on Daicel chiralpak OB-H or AD columns.

2.3.1.1. (4R)-Hydroxy-4-(2-nitrophenyl)-butan-2-one 1. Enantiomeric excess was determined by HPLC with a Daicel chiralpak OB-H column (i-PrOH/hexane = 15:85), 25 °C, 254 nm, 1 ml/min; major antienantiomer t_R 8.4 = min and minor antienantiomer t_R = 7.3 min. ^{1}H NMR ($CDCl_3$, 500 MHz): δ = 7.95–7.42 (m, 4H), 5.68 (d, J = 10.7 Hz, 1H), 3.73 (s, 1H), 3.15–2.72 (m, 2H), 2.24 (s, 3H).

2.3.1.2. (4R)-Hydroxy-4-(4-nitrophenyl)-butan-2-one 2. Enantiomeric excess was determined by HPLC with a Daicel chiralpak OB-H column (i-PrOH/hexane = 15:85), 25 °C, 254 nm, 1 ml/min; major antienantiomer t_R = 14.0 min and minor enantiomer t_R = 16.1 min. ^{1}H NMR ($CDCl_3$, 500 MHz): δ = 8.22–7.28 (m, 4H), 5.27 (s, 1H), 3.67 (s, 1H), 2.87 (d, J = 6.7 Hz, 2H), 2.23 (s, 3H).

Table 1
Chemical composition of different L-proline hybrids.

Entry	Samples	N content (wt.%)	L-proline content (mmol/g)	L-proline content (wt.%)
1	**L-proline/GO**	5.68	4.06	46.7
2	L-proline/AC	2.09	1.49	17.1
3	L-proline/Graphite	0.83	0.59	6.78

2.3.1.3. (4R)-Hydroxyl-4-(2-chlorophenyl)butan-2-one 3. Enantiomeric excess was determined by HPLC with a Daicel chiralpak AD column (i-PrOH/hexane = 7.5:92.5), 25 °C, 254 nm, 0.8 ml/min; major antienantiomer t_R = 10.9 min and minor antienantiomer t_R = 12.3 min. ^{1}H NMR (500 MHz, $CDCl_3$): δ = 7.61–7.18 (m, 4H), 5.52–5.49 (m, 1H), 3.63 (s, 1H), 3.00–2.65 (m, 2H), 2.21(s, 3H).

2.3.1.4. (4R)-Hydroxyl-4-(4-bromophenyl)butan-2-one 4. Enantiomeric excess was determined by HPLC with a Daicel chiralpak AD column (i-PrOH/hexane = 7.5:92.5), 25 °C, 254 nm, 0.8 ml/min; major antienantiomer t_R = 15.2 min and minor antienantiomer t_R = 16.1 min. ^{1}H NMR(500 MHz, $CDCl_3$): δ = 7.47–7.21 (m, 4H), 5.10 (t, J = 8.7 Hz, 1H), 3.43 (s, 1H), 2.86–2.76 (m, 2H), 2.19 (s, 3H).

2.3.1.5. (4R)-Hydroxyl-4-(4-acetamidophenyl)butan-2-one 5. Enantiomeric excess was determined by HPLC with a Daicel chiralpak AD column (i-PrOH/hexane = 10:90), 25 °C, 254 nm, 0.8 ml/min; major antienantiomer t_R = 50.0 min and minor antienantiomer t_R = 55.7 min. ^{1}H NMR(500 MHz, $CDCl_3$): δ = 7.47–7.26 (m, 4H,), 5.12–5.11 (m, 1H), 3.34 (s, 1H), 2.89–2.77 (m, 2H), 2.20 (s, 3H), 2.17 (s, 3H).

2.3.1.6. (4R)-Hydroxy-4-(2-naphthyl)butan-2-one 6. Enantiomeric excess was determined by HPLC with a Daicel chiralpak AD column (i-PrOH/hexane = 7.5:92.5), 25 °C, 254 nm, 0.8 ml/min; major antienantiomer t_R = 22.6 min and minor antienantiomer t_R = 27.0 min. ^{1}H NMR (500 MHz, $CDCl_3$): δ = 7.80–7.43 (m, 7H), 5.31–5.29 (m, 1H), 3.50 (s, 1H), 2.96–2.84 (m, 2H), 2.18 (s, 3H).

2.3.2. Typical procedure for the asymmetric aldol reactions of ketone with 2-nitrobenzaldehyde

A mixture of catalyst (0.035 g, 0.14 mmol L-proline content in the L-PROLINE/GO HYBRID) corresponding ketone (5 mmol) and DMSO (4 ml) was stirred at room temperature for 10 min. Subsequently, the 2-nitrobenzaldehyde (0.5 mmol) was added. The resulting mixture was stirred at room temperature until the reaction was judged to be complete based on TLC analysis. The reaction was quenched by adding saturated NH_4Cl solution, and then, the catalyst was separated by centrifugation. The products were extracted with Et_2O (3 × 5 ml), the combined extracts were dried over anhydrous Na_2SO_4, the solvent was evaporated in vacuo, and the residue was purified by column chromatography on silica gel (Acros, 40–60 μm, 60 Å, eluent *n*-hexane/EtOAc 3:1). The diastereoselectivity (dr) of aldols' products were measured by ^{1}H NMR of the crude reaction mixture. The enantioselectivity of the anti-isomers was determined by HPLC on Daicel chiralpak AD-H or AD column. The absolute configurations of the products were assigned by analogy with the previously reported results [28].

2.3.2.1. (3R,4S)-3-Methyl-4-hydroxy-4-(2-nitrophenyl)-butan-2-one 7. Enantiomeric excess for anti HPLC was determined by HPLC with a Daicel chiralpak AD-H column (i-PrOH/hexane = 15:85), 25 °C, 254 nm, 1.0 ml/min; major antienantiomer t_R = 7.3 min and minor antienantiomer t_R = 8.4 min. ^{1}H NMR ($CDCl_3$, 500 MHz): δ: anti: 7.95–7.42 (m, 4H), 5.40 (d, J = 9.8 Hz, 1H), 3.61 (s, 1H), 3.47–3.25 (m, 1H), 2.13 (s, 3H), 1.42–1.30 (m, 3H).

2.3.2.2. (2R,10S)-2-(Hydroxy-(2-nitrophenyl)methyl)cyclohexan-1-one 8. Enantiomeric excess for anti HPLC was determined by HPLC with a Chiralpak AD column (i-PrOH/hexane = 15:85), 25 °C, 254 nm, 1.0 ml/min, major antienantiomer t_R = 13.4 min, and minor antienantiomer t_R = 14.2 min. ^{1}H NMR (500 MHz, $CDCl_3$): δ: anti: 7.86–7.44 (m, 4H), 5.46–5.44 (d, J = 7.0 Hz, 1H), 2.47–2.44 (m, 1H), 2.49–2.34 (m, 2H), 2.09–2.08 (m, 1H), 1.87–1.66 (m, 6H).

2.3.2.3. (2R,10S)-2-(Hydroxy-(2-nitrophenyl)methyl)cyclopentan-1-one 9. Enantiomeric excess for anti HPLC was determined by HPLC with a Chiralpak AD column (i-PrOH/hexane = 10:90), 25 °C, 220 nm, 1.0 ml/min; major antienantiomer t_R = 15.5 min and minor antienantiomer t_R = 16.3 min. ^{1}H NMR (500 MHz, $CDCl_3$): δ: anti: 7.92–7.35 (m, 4H), 5.38–5.36 (d, J = 9.0 Hz, 1H), 2.79–2.74 (m, 1H), 2.34–2.28 (m, 1H), 2.13–2.05 (m, 2H), 1.99–1.95 (m, 1H), 1.69–1.62 (m, 4H).

3. Results and discussion

3.1. Preparation of the L-proline/GO hybrid

GO has a layered morphology with hydroxyl and epoxy groups functionality disrupting the hexagonal carbon basal planes on the interior of multilayered stacks of graphene oxide, and carboxyl groups decorating the periphery of the planes. The structural characteristics, together with its high-specific surface area, provide GO sheet with large capability of loading L-proline simply through non-covalent method. In addition, the mean interlayer distance between the GO sheet is reported to be in the range of 0.6–1.1 nm [33], which is far broader than the thickness of L-proline molecule (ca. 0.29 nm, reported in [23]), suggesting a flexible orientation of interlayer L-proline molecule in interlayer voids and the high accessibility of substrates. Base on the specific physicochemical properties of GO, we try to prepare the heterogeneous **L-proline/GO** hybrid catalyst by intercalating the L-proline into the GO interlayer galleries. A strategy that we have designed here is to maintain the pristine L-proline backbone, since both the carboxylic acid and the pyrrolidine functionalities are essential for effective asymmetric induction. The **L-proline/GO** hybrid was prepared simply by mixing the GO sheet with pristine L-proline in aqueous solution, where the hydrogen-bonding interaction between hydroxyl and epoxyl groups on the GO sheet with carboxyl and secondary amine groups in L-proline could be formed during the preparation procedure. Therefore, the driving force for L-proline binding to the GO sheet should be primarily attributed to hydrogen-bonding interaction, which occurs on the basal planes existing in the interlayer of the GO minerals. Also, the ionic interaction may also occur at the carboxylic group sites on the edge of layered mineral, which was proposed in Scheme 1. In order to investigate the interaction between L-proline and GO sheet, other carbonaceous supports with less oxygen functional groups, such as active carbon and graphite, were employed for the L-proline loading. It is found that the loading of L-proline on GO (as high as 4.06 mmol/g) is much higher than that on the active carbon (1.49 mmol/g) and on the graphite (0.59 mmol/g) (Table 1, entry 1 vs. 2, 3). It is suggested that the presence of the abundant oxygen functional groups on the planar surface or edge of GO sheet, as well as the high efficient utilization of the surface area of the GO sheet, is responsible for the higher L-proline loading on GO sheet.

3.2. Samples characterization

3.2.1. AFM

We employed AFM to establish the thickness and surface roughness of the **L-proline/GO** hybrid since AFM characterization

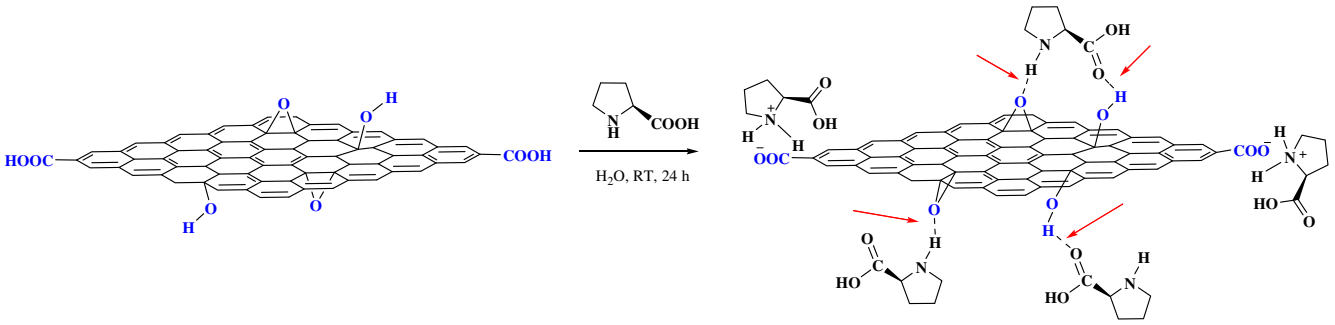

Scheme 1. Illustration of the preparation of L-**proline/GO** hybrid. The red arrows demonstrate hydrogen bonds. (For interpretation of the references to color in this figure legend, the reader is referred to the web version of this article.)

has been one of the most direct methods of probing the loading of organic molecular on GO sheets by quantifying the thickness of the sheets after they dispersed in a solvent. Fig. 1 shows the AFM image of L-**proline/GO** hybrid. The sample used for AFM study was prepared by depositing the hybrid on new cleaved mica surfaces and dried at room temperature. It is found that sufficiently dilute suspensions of the sample prepared with the aid of ultrasound results in the exfoliated L-**proline/GO** hybrid. The average thickness of the as-prepared L-**proline/GO** hybrid measured from the height profile of the AFM image is *ca.* 2.0 nm, being somewhat larger than the typical thickness of the single-layer GO (*ca.* 1.4 nm) [24]. An increase in the thickness (*ca.* 0.6 nm) of L-**proline/GO** hybrid may arise from a certain content of L-proline molecules loaded onto the GO surface. If we assume that monolayered L-proline molecules cover both sides of GO sheet, the estimated thickness of the monolayered L-proline molecules is *ca.* 0.30 nm. This value is in agreement with to the reported thickness of L-proline molecule (*ca.* 0.29 nm) [23]. We thus propose that the monolayered L-proline molecules are loaded on both sides of GO sheet without aggregation, although the distinct L-proline molecules are not observed on the plain GO sheets in the AFM image. On the other hand, the cross-sectional view of the sheets displays the slight height variations of about 0.2–0.3 nm, which further confirms the load of the monolayered L-proline on the GO sheet. Furthermore, the height of the sample shows another obvious stage with the increment of 3.0 nm, corresponding to the labeled distinct light "bulge" in the AFM image of the L-**proline/GO** hybrid. Based on the multilayered structure of the L-**proline/GO** hybrid, it is believed that the light "bulge" should be the accumulated hybrid sheet. Accordingly, the interlayer spacing of the L-**proline/GO** hybrid can be derived to be *ca.* 1.0 nm. The layered structure of the L-**proline/GO** hybrid is also confirmed by XRD pattern.

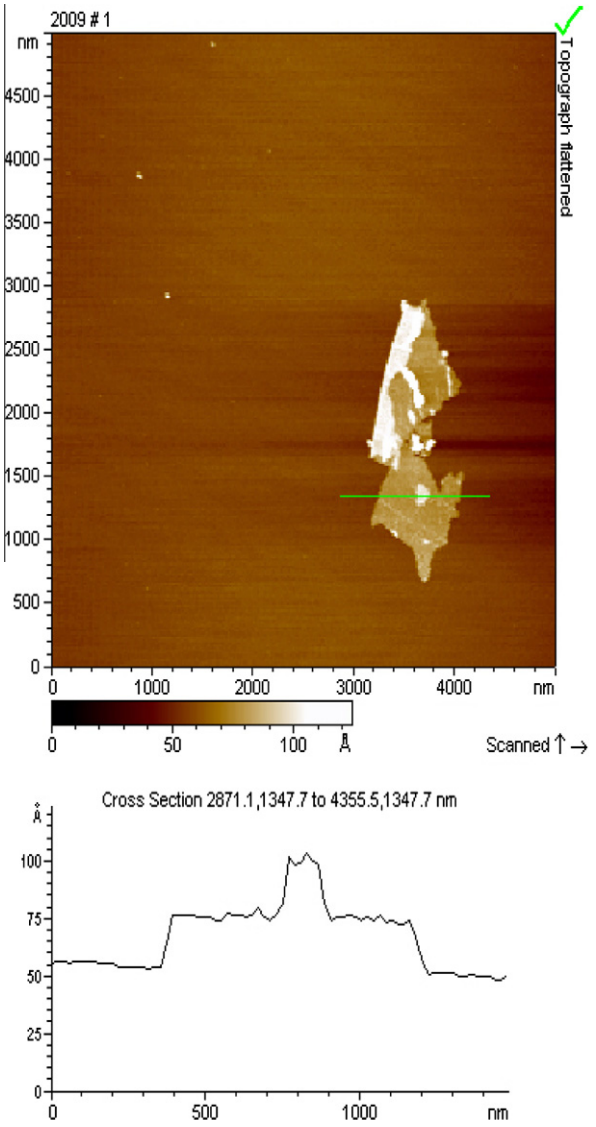

Fig. 1. AFM image of L-**proline/GO** hybrid on freshly cleaved mica, with a concentration of 0.01 mg/ml in water.

3.2.2. XRD

XRD patterns are used to study the change of GO sheet in structure during the loading process. Fig. 2 shows powder XRD results of GO material, L-proline, and L-**proline/GO** hybrid. XRD pattern of GO shows a very strong (002) peak (denoted as #, 2θ) centered at 9.4°, corresponding to an average interlayer distances of *ca.* 0.95 nm (Fig. 2a). Notably, as for L-**proline/GO** hybrid, the C (002) peak (denoted as #, 2θ) shifts to 8.9° (Fig. 2b), corresponding to a larger interlayer distance of *ca.* 0.99 nm. The value is approach to that determined by AFM (1.0 nm). The larger interlayer spacing suggests the intercalation of L-proline into the interlayer spacing of multilayered GO material during the loading process as opposed to simple absorption on the external surface. In addition to the C (002) peak (2θ) at 8.9°, the main intense diffraction peaks of pristine L-proline (denoted as *) based on the standard spectrum are also observed in the XRD pattern of L-**proline/GO** hybrid due to the presence of the L-proline on the GO sheet (Fig. 2b vs. c). The intercalation of L-proline into the GO interlayer galleries provides a sandwich-like hybrid material where layers of GO sheet alternate with layers of L-proline. The substrates thus can easily access to the active sites in the gallery regions, which allows the heterogeneous

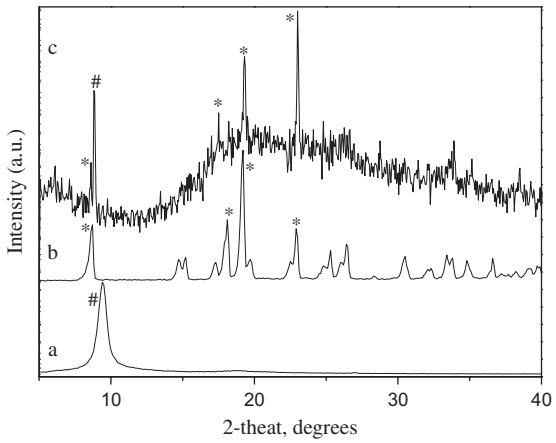

Fig. 2. XRD patterns of the samples of GO (a), L-proline (b) and **L-proline/GO** (c).

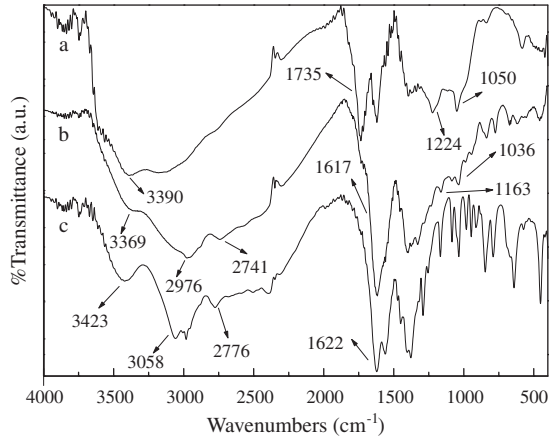

Fig. 3. FT-IR spectra of GO (a), **L-proline/GO** (b) and pristine L-proline (c).

L-proline/GO catalyst to perform as the homogeneous catalyst in the direct asymmetric aldol reaction.

3.2.2. FT-IR

The binding behavior of pristine L-proline toward GO can be confirmed by characterizing the GO sheet, hybrid material of **L-proline/GO**, and pristine L-proline using FT-IR spectroscopy, as shown in Fig. 3. The FT-IR spectrum of GO shows characteristic vibration bands of oxygen-containing groups at round 3390, 1735, 1224, and 1050 cm^{-1}, which are associated with the stretching vibration modes of COO—H/O—H, carboxylic C=O, C—OH, and epoxy C—O groups present on the surface of GO, respectively (Fig. 3a) [34,35]. While, the wavenumber of the characteristic band of the oxygen functional groups decreases from 3390, 1224, and 1050 cm^{-1} to 3369, 1163, and 1036 cm^{-1}, respectively, after forming **L-proline/GO** hybrid, except for the band corresponding to ν(C=O) in the spectrum of GO sheet. The observation indicates that L-proline is successfully loaded onto GO, and the shift of characteristic bands may be due to the hydrogen-bonding interaction between these two species (Fig. 3b vs. a). The deduction also can be drawn from the evidence that the absorption band assigning to the —COOH group in pristine L-proline, shifts from 1622 to 1617 cm^{-1}, compared with that of **L-proline/GO** hybrid (Fig. 3c vs. b). In addition, the bands at 2776 cm^{-1} corresponding to the asymmetric stretching vibration of the N—H group in L-proline [23] are also found to shift to a lower position at 2741 cm^{-1}, due to the formation of hydrogen bond between secondary amine group

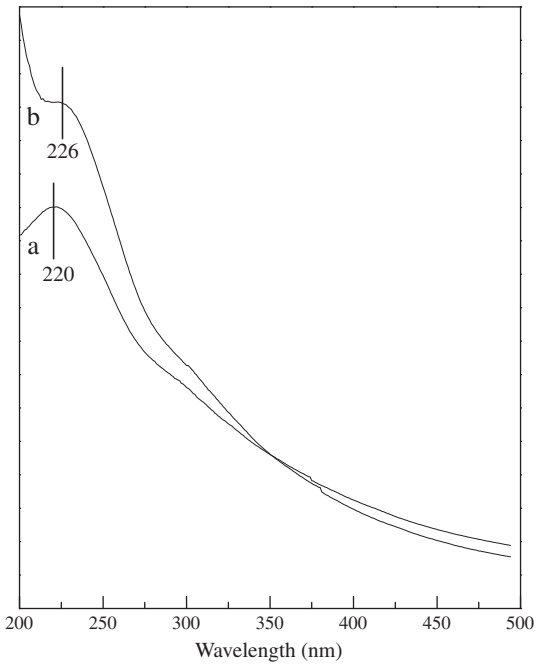

Fig. 4. UV–vis spectra of GO (a) and **L-proline/GO** (b) in aqueous solution.

(—NH—) of L-proline and the oxygen functional groups of GO sheet (Fig. 3c vs. b). Furthermore, the characteristic band at 1735 cm^{-1} relating to the ν(C=O) of carboxyl group in the spectrum of GO sheet disappeared after the L-proline is loaded (Fig. 3b vs. a), providing the existence of ionic interaction between the $—NH_2^+—$ group and the $—COO^-$ group originated from the reaction between the secondary amine group (—NH—) of L-proline and the carboxylic group (—COOH) on the edge of GO sheet [36]. All the results encourage us to anticipate that the pristine L-proline bind to the planar surface or edge of GO sheet through hydrogen-bonding or/and ionic interaction, respectively.

3.2.3. UV–vis

UV–visible absorption spectra of pure GO and **L-proline/GO** hybrid in aqueous solution furthermore verified the interaction between GO and L-proline, as described in Fig. 4. It was obvious that the GO exhibits a maximum absorption at 220 nm, which corresponds to $\pi \rightarrow \pi^*$ transitions of aromatic C=C bonds. The characteristic peak shows a redshift to 226 nm in the UV–vis spectrum of **L-proline/GO** hybrid. The slight redshift relative to GO suggests that the presence of the ground-state electron donor–acceptor interaction between the GO and L-proline in the **L-proline/GO** hybrid [29,37].

3.2.4. TG–DTG

Thermogravimetric analysis (TGA) associated with the decomposition profiles of the GO, L-proline, and **L-proline/GO** hybrid under a nitrogen atmosphere provides further evidence for the intercalation of L-proline into the GO interlayer galleries, as well as the presence of hydrogen-bonding interaction between L-proline molecular and GO sheet, as shown in Fig. 5. Pure GO sheet shows the main weight loss centered at 160 °C, which is presumably due to pyrolysis of the labile oxygen-containing functional groups (Fig. 5a) [38]. Fig. 5b displays the TG–DTG curves of **L-proline/GO** hybrid. Obviously, the decomposition temperature of the oxygen-containing functional groups decreased to 140 °C after the L-proline loading. It is probably attributed to the extended interlayer distance originated from the intercalation of L-proline, which

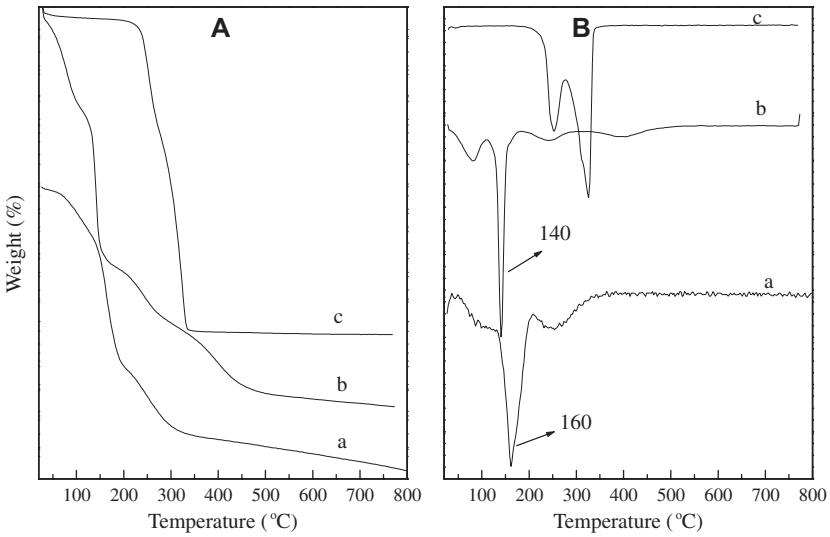

Fig. 5. Thermogravimetric (A) and differential thermogravimetric (B) results of the GO (a), L-**proline/GO** (b) and pristine L-proline (c) under a nitrogen atmosphere.

reduces the interlayer interaction forces between GO nanosheets and further reduces thermal stability of the oxygen-containing functional groups [39]. Moreover, the temperature of the successive pyrolysis of the L-proline moiety in the **L-proline/GO** hybrid gets increased comparing with that of the pristine L-proline. It is an indirect proof for the presence of hydrogen-bonding interaction between L-proline molecular and the oxygen-containing functional groups of GO sheet in the **L-proline/GO** hybrid (Fig. 5b vs. c).

To the detailed study, the relationship between the oxygen-containing functional groups GO sheet and L-proline loading, TGA was further performed to monitor the decomposition profile of the pristine L-proline and **L-proline/GO** hybrid under air atmosphere. For comparison, the control catalysts of L-proline/AC and L-proline/graphite are also characterized by means of the TG-DTG under air atmosphere, and the results obtained are depicted in Fig. 6. The pristine L-proline shows two distinct steps of weight loss in the combined TG–DTG curves (Fig. 6A). The first weight loss centers at 68 °C, which is due to a loss of water. The second large weight loss assigned to the successive cleavage of the L-proline appears at 215 °C. The weight loss extends up to ca. 585 °C until the L-proline is completely decomposed under air flow. Fig. 6B displays the TG–DTG curves of **L-proline/GO** hybrid, in which three major steps are observed. The first step (weight loss = ca. 10 wt.%) before 100 °C corresponds to removal of the surface-adsorbed water and interlayer water molecules. The second step involves the weight loss centered at 131 °C and the followed weight loss at 220 °C. The two weight loss peaks are well distinguished in the corresponding DTG curve, which are logically assigned to the successive pyrolysis of the labile oxygen-containing functional groups (weight loss = ca. 23 wt.%). It is the presence of the abundant oxygenated species responsible for the highly efficient loading of L-proline. The third step, in the temperature range of 317–780 °C, is logical to assign to the successive cleavage of the L-proline moiety [23], since the weight loss in this range (ca. 46 wt.%) is approximate to the content of L-proline moiety calculated from the elemental analysis (46.7 wt.%). The increased decomposition temperature of the L-proline suggests that the guest/host interaction was done through the oxygen-containing functional groups of the GO sheet (Scheme 1). Therefore, we can deduce that the L-proline is successfully loaded on the GO sheet by forming the non-covalent bond rather than physical adsorption. The non-removable residue is probably belonged to the remaining carbon. The control catalysts of L-proline/AC and L-proline/graphite also show the three-step decomposition profiles in the corresponding TG–DTG curves (Fig. 6C and D), corresponding to the removal of water (first step in the range of 46–100 °C), pyrolysis of oxygen-containing groups (second step in the range of 112–237 °C), and the decomposition of L-proline moiety (third step in the range of 254–533 °C). Thus, the mass percentage of the oxygen-containing groups (ca. 7.0 wt.%) and the L-proline moiety (ca. 16 wt.%) in the L-proline/AC hybrid can be estimated according to the weight loss of corresponding decomposition range (Fig. 6C). The contents of the oxygen-containing groups and the L-proline moiety in the L-proline/graphite hybrid are estimated to be 1 and 7 wt.%, respectively (Fig. 6D). The L-proline content estimated according to the TG data is close to those calculated from the nitrogen elemental analysis (see Table 1). Notably, higher content of the oxygen-containing groups gives rise to higher loading of L-proline for the supported catalysts. The results provide supporting evidence that the high-efficiency loading of L-proline depends on the amount of the oxygenated groups in the support. The high loading of L-proline on the GO sheet, together with the unique binding behaviors between L-proline and GO sheet, makes the L-proline/GO hybrid efficient and stable in the reaction system.

3.3. Catalytic performance

Apart from the ultrahigh loading capacity of GO sheet toward L-proline, the other salient feature of the **L-proline/GO** hybrid material is the efficient utilization of active sites because all the active sites located on the surface of the layer are accessible, which will render the **L-proline/GO** hybrid efficient for the direct asymmetric aldol reaction. The catalytic efficiency of the resultant **L-proline/GO** hybrid catalyst was investigated using the direct asymmetric aldol reaction of 2-nitrobenzaldehyde and acetone at room temperature. The results are presented in Table 2. The GO material and pristine L-proline were also examined for comparison purposes.

GO material itself was found to be inactive for the direct asymmetric aldol reaction, and practically, no aldol product was acquired even if 0.035 g GO sheet was used (Table 2, entry 1). When pristine L-proline was employed in 30 mol% catalyst loading, the aldol product was isolated in a chemical yield (95%) and an *ee* value (79%) (Table 2, entry 2). In general, the immobilization of the homogeneous catalyst causes a decrease in the catalytic activity. However, the immobilization of L-proline on GO sheet *via*

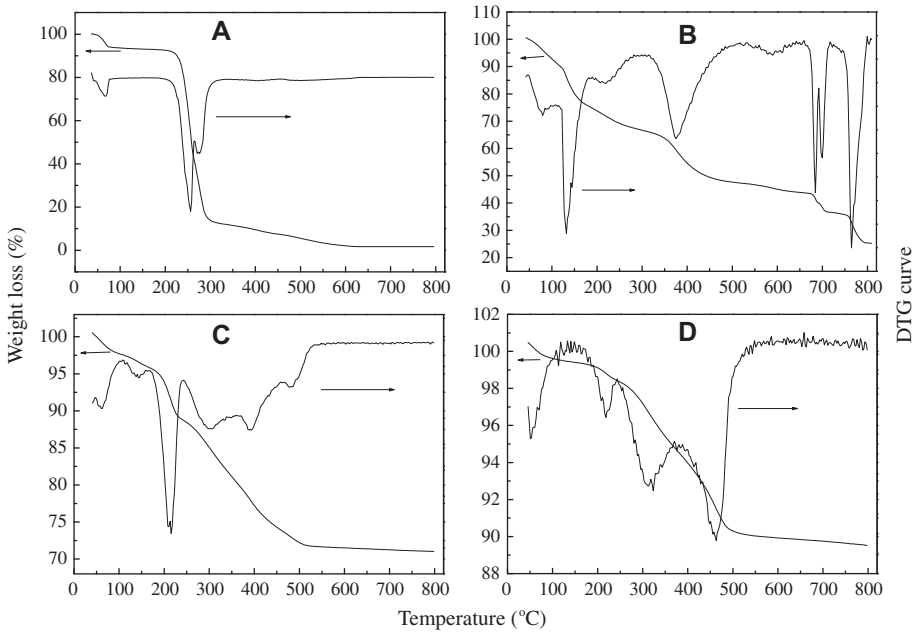

Fig. 6. TG–DTG results of the L-proline (A), **L-proline/GO** (B), L-proline/AC (C) and L-proline/graphite (D) under an air atmosphere.

Table 2
The results of the direct asymmetric aldol reaction between acetone and 2-nitrobenzaldehyde over different L-proline catalysts.[a]

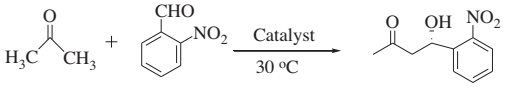

Entry	Catalyst	Catalyst amount (g)	Time (h)	Yield[b] (%)	*Ee*[c] (%)
1	GO	0.035	24	Trace	n.d.[d]
2	Pristine L-proline	0.017[e]	6	95	79
3	**L-proline/GO**	0.035[e]	6	96	79
4	**L-proline/GO**	0.025	24	95	79
5	**L-proline/GO**	0.012	48	95	78
6	L-proline/AC	0.035	24	10	n.d.[d]
7	L-proline/Graphite	0.035	24	trace	n.d.[d]

[a] Reaction conditions: 2-nitrobenzaldehyde (0.5 mmol), acetone (4 ml), 30 °C.
[b] Isolated yield after column chromatography.
[c] *Ee* was determined by HPLC (Daicel chiralpak OB-H column) on pure products.
[d] Not determined.
[e] The amount of catalyst is 30 mol% of 2-nitrobenzaldehyde.

hydrogen-bonding or/and ionic interaction has no adverse effect on the catalytic activity of L-proline in the asymmetric aldol reaction. In particular, the hydrogen-bonding interaction between the carboxyl group (—COOH) of L-proline and the hydroxyl (—OH) group of GO sheet makes the proton of the carboxyl (—COOH) group more acidic, which is favorable for the direct asymmetric aldol reaction present here [5,40–44]. The isolated yield and *ee* value for the **L-proline/GO** hybrid could be comparable to those observed by using pristine L-proline at the same catalyst loading (30 mol%) under the identical conditions (yield of 96% and *ee* of 79%) (Table 2, entry 3 vs. 2). The high efficiency of the heterogeneous catalyst might be due to the unique multilayered structure of the GO carrier, which provided both stable anchoring site for active sites and accessible void for reagents. Furthermore, L-proline, intercalated in the GO material, could be used as stabilizer for dispersing **L-proline/GO** sheet in the reaction system [45]. The high accessibility of substrate to active sites, as well as the well dispersion of **L-proline/GO** in reaction system, allowed the heterogeneous catalyst to behave as a homogeneous catalyst. A reduction in the amount of catalyst to 0.025 g (which amounts to 20 mol%, regarding catalytic L-proline sites), or further to 0.012 g (which amounts to 10 mol%, regarding catalytic L-proline sites), resulted in a relatively slow reaction but still gave quantitative yield and 79% *ee* within 48 h (Table 2, entries 4 and 5).

The catalytic activities are also correlated in detail with the amount of loaded L-proline. Both L-proline/AC hybrid and L-proline/graphite hybrid with low L-proline loading gave small amount of aldol product in control experiments, even though their dosages (0.035 g) were identical with that of the **L-proline/GO** (Table 2, entries 6 and 7). The results suggested that the layered GO sheet with the unique basal plane structure, together with the abundant oxygen functional groups, was the optimal carrier for L-proline, which provided the **L-proline/GO** with large L-proline loading and high efficiency.

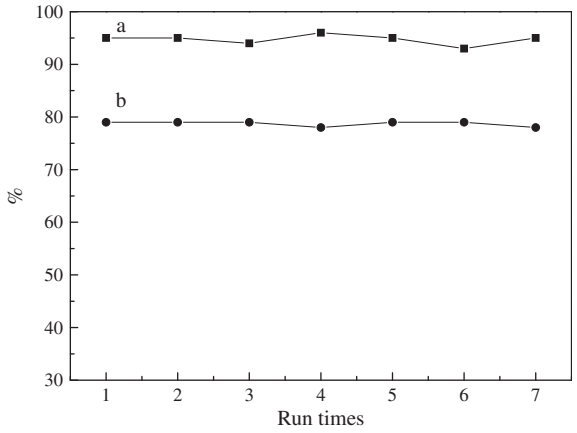

Fig. 7. The reuse of L-**proline/GO** in the direct asymmetric aldol reaction between acetone and 2-nitrobenzaldehyde at 30 °C (a: yield; b: ee value).

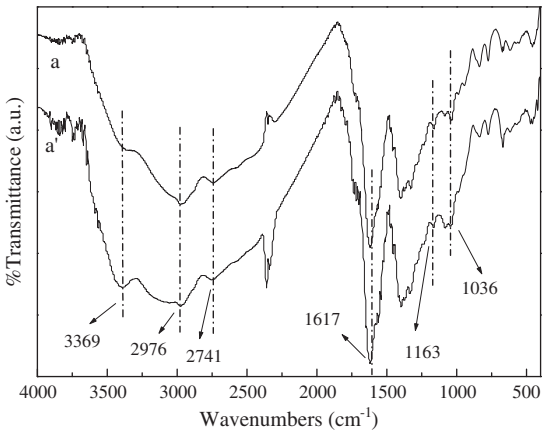

Fig. 8. FT-IR spectra of the fresh L-**proline/GO** catalyst (a) and the recovered L-**proline/GO** after the 7th reuse (a').

3.4. Recycling

Binding of L-proline to the edge and plane of GO sheet makes the L-**proline/GO** hybrid stable in the reaction system. After the reaction, the heterogeneous L-**proline/GO** catalyst could be facilely separated from the reaction mixture by centrifugation. The upper organic phase with the product was separated from the lower catalyst by simple decantation. The recovered catalyst was washed with ethyl acetate and dried at 40 °C overnight for reused.

Fig. 7 showed the results of the recovery and reusability of the L-**proline/GO** hybrid. To our delight, the L-**proline/GO** hybrid could be reused for seven times with no appreciable decrease in yield and enantioselectivity of aldol product, which demonstrated the prepared L-**proline/GO** catalyst possess excellent stability and reusability. The reaction was completely stopped by the removal of the catalyst. Elementary analysis of the recovered catalyst was used for determining the L-proline leaching in terms of nitrogen element percentage, and there were no significant changes in the nitrogen element percentage compared with the fresh catalyst. The inactivity of supernatants, as well as the maintaining of nitrogen element percentage in the L-**proline/GO** catalyst, indicated that any leaching of active species into solution was insignificant. Further evidence of the stability of the heterogeneous catalyst was provided by the FT-IR spectra of the L-**proline/GO** hybrid with fresh and reused for seven times (Fig. 8a vs. a'). No significant changes of the catalyst took place even after reuse for seven times. These observations suggested that the efficient L-**proline/GO** catalyst was perfectly stable during the direct asymmetric aldol reaction presented here and was readily recyclable from the reaction system. Notably, the recycle of the pristine L-proline resulted in a significant decrease in activity (from 95% to 65% yield in the second cycle) with no change of the *ee* value (79%) due to the problem of quantitative recovery.

3.5. The asymmetric aldol reactions of ketone with various aryl aldehydes

Application scope of the catalytic system was then examined under the optimized conditions, and the results are summarized in Table 3. A wide range of aromatic aldehydes bearing either electron-rich or electron-deficient substitutes underwent reaction with acetone to produce the corresponding β-hydroxy ketone in moderate to high yield and enantioselectivity at room temperature. The electron nature and steric hindrance of the substituents on the aromatic aldehydes affected the yield of the corresponding aldol products dramatically. In general, the reaction between acetone and aromatic aldehydes bearing electron-withdrawing groups on the aromatic ring furnished the desired β-hydroxy carbonyl aldol products in excellent yields (in the range of 66–95%) within 6 h (Table 3, entries 1–2). The halogenated aromatic aldehydes could be employed even though longer reaction times were generally required (Table 3, entries 3–4). The 4-acetamidobenzaldehyde used as an electron-rich aromatic aldehyde showed the moderate reactivity with the presence of 30 mol% of catalyst (Table 3, entry 5). The 2-naphthaldehyde was also found to be less reactive due to the 2-naphthyl group, which was unfavorable for nucleophilic attack due to steric hindrance (Table 3, entry 6). Obviously, the electronic nature of substituents did not show much influence on the enantioselectivity, and the stereochemical outcome of the condensation was regulated by the proline residue. While the nitro group located at ortho position seemed to play an important role in helping the stereocontrol of the condensation. The *ee* value of the 4-hydroxy-4-(2-nitrophenyl)-butan-2-one was slightly higher than other aldol products even though all of the aromatic aldehydes afforded the same major enantiomer of the β-hydroxy ketone (Table 3, entry 2 vs. 1). Therefore, 2-nitrobenzaldehyde was chosen as the model to check the feasibility of using other ketones as aldol donors in the direct asymmetric aldol reaction.

Given the scope of ketone, butanone, cyclohexanone, and cyclopentanone as aldol donors were also investigated into the direct asymmetric reaction with 2-nitrobenzaldehyde. The results are summarized in Table 4. The butanone exhibited the similar activity as the acetone and provided almost quantitative yield of aldol product (up to 92%), as shown in Table 4 (Table 4, entry 2 vs. 1). While, different from the acetone, butanone as the aldol donor produced two different aldol products due to the presence of two different α-carbon centers in the butanone. The desired product of (3R,4S)-3-methyl-4-hydroxy-4-(2-nitrophenyl)-butan-2-one was obtained in only 35% yield with the lower diastereoselectivity of 59:41 (*anti*/*syn*), and the enantioselectivity of the anti-isomer was 86% (Table 4, entry 2). We also examined the feasibility of using cyclic ketones, such as cyclohexanone and cyclopentanone, as aldol donors. Although a longer reaction time was required in comparison with acyclic ketones, satisfactory results were obtained. Cyclohexanone reacted with 2-nitrobenzaldehyde to generate aldol adduct in a high yield (up to 96%) with an excellent dr of 93:7 (*anti*/*syn*). The *ee* value for the anti-isomer was 92% (Table 4, entry 3). In the case of cyclopentanone, similarly, high yield of 93% was isolated within 8 h, while the dr and *ee* values of aldol were somewhat lower (Table 4, entry 4 vs. 3).

Table 3
The direct asymmetric aldol reaction between acetone and aromatic aldehydes catalyzed by L-**proline/GO**.[a]

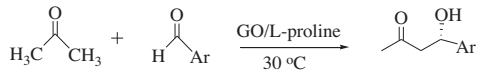

Entry	Ar	Product	Reaction time (h)	Yield (%)[b]	*Ee* (%)
1	2-$NO_2C_6H_4$	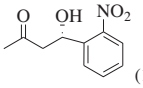 (1)[c]	6	96	79
2	4-$NO_2C_6H_4$	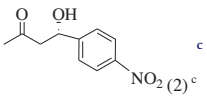 (2)[c]	6	95	68
3	2-ClC_6H_4	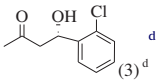 (3)[d]	12	91	66
4	4-BrC_6H_4	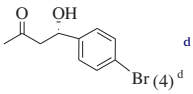 (4)[d]	24	66	63
5	4-$AcNHC_6H_4$	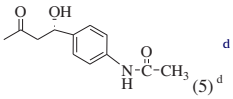 (5)[d]	24	43	55
6	2-Naphthyl	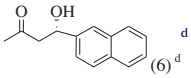 (6)[d]	24	56	55

[a] Reaction conditions: L-**proline/GO** (0.035 g, 30 mol% of aromatic aldehydes), aromatic aldehydes (0.5 mmol), acetone (4 ml), 30 °C.
[b] The same as Table 2.
[c] *Ee* was determined by HPLC (Daicel chiralpak OB-H column) on pure products.
[d] *Ee* was determined by HPLC (Daicel chiralpak AD column) on pure products.

Table 4
The direct asymmetric aldol reaction between ketones and 2-nitrobenzaldehyde catalyzed by L-**proline/GO**.[a]

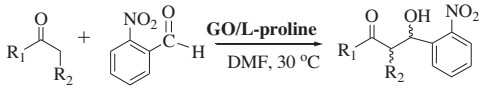

Entry	Product	Reaction time (h)	Yield (%)[b]	dr(*anti*/*syn*)[c]	*Ee* (%)
1	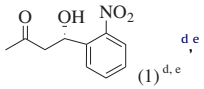 (1)[d,e]	6	96	/	79
2	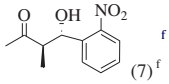 (7)[f]	5	35 (92)[g]	59:41	86
3	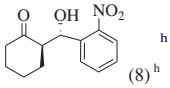 (8)[h]	24	96	93:7	92
4	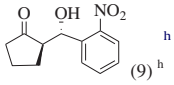 (9)[h]	8	93	83:17	89

[a] Reaction conditions: L-**proline/GO** (0.035 g, 30 mol% of 2-nitrobenzaldehyde), 2-nitrobenzaldehyde (0.5 mmol), ketone (5 mmol), DMSO (4 ml), 30 °C.
[b] The same as Table 2.
[c] Determined by ^{1}H NMR analysis, major product is anti.
[d] Reaction conditions: L-**proline/GO** (0.035 g, 30 mol% of aromatic aldehydes), aromatic aldehydes (0.5 mmol), acetone (4 ml), 30 °C.
[e] *Ee* was determined by HPLC (Daicel chiralpak OB-H column) on pure products.
[f] *Ee* was determined by HPLC (Daicel chiralpak AD-H column) on the anti-product.
[g] Only the regioisomer as shown was obtained. The total yield of isolated aldol products is given in parentheses.
[h] *Ee* was determined by HPLC (Daicel chiralpak AD column) on the anti-product.

4. Conclusions

The unique layered GO material was shown to be a suitable support for the highly efficient loading of L-proline through a simple non-covalent method to afford a layered **L-proline/GO** hybrid catalyst for the direct asymmetric aldol reaction. Technologies of characterization of AFM, XRD, FT-IR, UV–vis, and TGA results confirmed the loading of L-proline on the two sides and edge of the GO sheet through hydrogen-bonding or/and ionic interaction. The obtained **L-proline/GO** hybrid provided relevant aldol products in yield and enantioselectivity comparable to those observed in the reactions promoted by L-proline itself. Furthermore, the heterogeneous catalyst was stable in the reaction system and could be easily recovered from the reaction mixture.

Acknowledgments

The project was financial supported by the National Natural Science Foundation of China (Grant Nos. 21003044, 20973057), the Natural Science Foundation of Hunan Province (10JJ6028) and the Program for Science and Technology Innovative Research Team in Higher Educational Institutions of Hunan Province.

References

[1] E.R. Jarvo, S.J. Miller, Tetrahedron 58 (2002) 2481.
[2] K. Nakamura, R. Yamanka, T. Matsuda, T. Harada, Tetrahedron: Asymmetry 14 (2003) 2659.
[3] W. Hotz, F. Tanaka, C.F. Barbas III, Acc. Chem. Res. 37 (2004) 580.
[4] S. Mukherjee, J.W. Yang, S. Hoffmann, B. List, Chem. Rev. 107 (2007) 5471.
[5] B. List, R.A. Lerner, C.F. Barbas, J. Am. Chem. Soc. 122 (2000) 2395.
[6] S. Luo, X. Mi, S. Liu, H. Xua, J. Cheng, Chem. Commun. (2006) 3687.
[7] N. Zotova, A. Franzke, A. Armstrong, D.G. Blackmond, J. Am. Chem. Soc. 129 (2007) 15100.
[8] G. Chen, X. Fu, C. Li, C. Wu, Q. Miao, J. Organomet. Chem. 702 (2012) 19.
[9] M. Gruttadauria, F. Giacalone, A.M. Marculescu, R. Notoa, Adv. Synth. Catal. 350 (2008) 1397.
[10] M. Gruttadauria, A.M.P. Salvo, F. Giacalone, P. Agrigento, R. Noto, Eur. J. Org. Chem. 2009 (2009) 5437.
[11] S. Calogero, D. Lanari, M. Orrù, O. Piermatti, F. Pizzo, L. Vaccaro, J. Catal. 282 (2011) 112.
[12] J. Zou, W. Zhao, R. Li, H. Zhang, Y. Cui, J. Appl. Polym. Sci. 118 (2010) 1020.
[13] A. Lu, T.P. Smart, T.H. Epps, D.A. Longbottom, R.K. ÓReilly, Macromolecules 44 (2011) 7233.
[14] S.J. Bae, S.W. Kim, T. Hyeon, B.M. Kim, Chem. Commun. (2000) 31.
[15] A. Zamboulis, N.J. Rahier, M. Gehringer, X. Cattoën, G. Niel, C. Bied, J.J.E. Moreau, M.W.C. Man, Tetrahedron: Asymmetry 20 (2009) 2880.
[16] F. Calderón, R. Fernndez, F. Snchez, A. Fernndez-Mayoralas, Adv. Synth. Catal. 347 (2005) 1395.
[17] E.G. Doyagüez, F. Calderon, F. Sanchez, A. Fernndez-Mayoralas, J. Org. Chem. 72 (2007) 9353.
[18] W. Miao, T.H. Chan, Adv. Synth. Catal. 348 (2006) 1711.
[19] S. Luo, X. Mi, L. Zhang, S. Liu, H. Xu, J. Cheng, Angew. Chem. Int. Ed. 45 (2006) 3093.
[20] J. Huang, X. Zhang, D.W. Armstrong, Angew. Chem. Int. Ed. 46 (2007) 9073.
[21] J. Li, G. Yang, Y. Qin, X. Yang, Y. Cui, Tetrahedron: Asymmetry 22 (2011) 613.
[22] H. Yang, S. Li, X. Wang, F. Zhang, X. Zhong, Z. Dong, J. Ma, J. Mol. Catal. A 363–364 (2012) 404.
[23] Z. An, W. Zhang, H. Shi, J. He, J. Catal. 241 (2006) 319.
[24] Y. Xu, H. Bai, G. Lu, C. Li, G. Shi, J. Am. Chem. Soc. 130 (2008) 5856.
[25] C. Petit, T.J. Bandosz, Adv. Funct. Mater. 20 (2010) 111.
[26] K. Nikolaos, P.E. Solon, S. Evangelia, T. Nikos, Carbon 48 (2010) 854.
[27] X. Hu, L. Mu, J. Wen, Q. Zhou, Carbon 50 (2012) 2772.
[28] A.R. Siamaki, A.E.R.S. Khder, V. Abdelsayed, M.S. El-Shall, B.F. Gupton, J. Catal. 279 (2011) 1.
[29] X. Yang, X. Zhang, Z. Liu, Y. Ma, Y. Huang, Y. Chen, J. Phys. Chem. C 112 (2008) 17554.
[30] R. Nie, J. Wang, L. Wang, Y. Qin, P. Chen, Z. Hou, Carbon 50 (2012) 586.
[31] Y. Chi, S.T. Scroggins, E. Boz, J.M.J. Fréchet, J. Am. Chem. Soc. 130 (2008) 13287.
[32] W.S. Hummers Jr., R.E. Offeman, J. Am. Chem. Soc. 80 (1958) 1339.
[33] N.V. Medhekar, A. Ramasubramaniam, R.S. Ruoff, V.B. Shenoy, ACS Nano. 4 (2010) 2300.
[34] Y.C. Si, E.T. Samulski, Nano. Lett. 8 (2008) 1679.
[35] A.J. Patil, J.L. Vickery, T.B. Scott, S. Mann, Adv. Mater. 21 (2009) 3159.
[36] K. Su, T. Pa, Y. Zhang, The Analytic Method of Spectrum, East China University of Science & Technology Press, Shanghai, 2002. 100.
[37] D. Depan, J. Shah, R.D.K. Misra, Mater. Sci. Eng. C 31 (2011) 1305.
[38] X. Tang, W. Li, Z. Yu, M.A. Rafiee, J. Rafiee, F. Yavari, N. Koratkar, Carbon 49 (2011) 1258.
[39] Q. Zhang, W. Li, T. Kong, R. Su, N. Li, Q. Song, M. Tang, L. Liu, G. Cheng, Carbon, 2012. http://dx.doi.org/10.1016/j.carbon.2012.08.025.
[40] Ö. Reis, S. Eymur, B. Reis, A.S. Demir, Chem. Commun. (2009) 1088.
[41] J.N. Moorthy, S. Saha, Eur. J. Org. Chem. 3864 (2006) 3864.
[42] Z. Tang, Z. Yang, X. Chen, L. Cun, A. Mi, Y. Jiang, L. Gong, J. Am. Chem. Soc. 127 (2005) 9285.
[43] D. Gryko, R. Lipi'nski, Adv. Synth. Catal. 347 (2005) 1948.
[44] Y. Zhou, Z. Shan, J. Org. Chem. 71 (2006) 9510.
[45] H. Bai, C. Li, G. Shi, Adv. Mater. 23 (2011) 1089.